Adaptive Control of a Recompression Four-Cylinder HCCI Engine

Jacob Larimore, *Student Member, IEEE*, Shyam Jade, *Student Member, IEEE*, Erik Hellström, *Member, IEEE*, Li Jiang, and Anna G. Stefanopoulou, *Fellow, IEEE*

***Abstract*— An adaptive controller is presented for the control of combustion phasing in a multicylinder homogeneous charge compression ignition engine. Adaptive parameter estimation is used to modify a model-based feedforward controller for each cylinder's start of injection (SOI) timing in an effort to mitigate model errors and increase the feedforward control accuracy. In-cylinder pressure measurements are used to calculate combustion phasing, which is compared with the prediction of an online nonlinear engine model to drive the parameter estimation that adapts the feedforward controller. It is demonstrated through experiments that the adaptive parameter can reduce the parameterization effort by allowing the model to adapt and match the response of each cylinder. It is also shown that the adaptive feedforward control is more accurate in the sense that load transitions can be achieved with less correction from the feedback controller. Overall, an average reduction of 41% in the absolute value of the SOI feedback component at steady state is achieved.**

***Index Terms*— Adaptive control, adaptive estimation, internal combustion engines, linear feedback control systems, nonlinear dynamical systems, power-train control.**

NOMENCLATURE

m_f	Fuel mass per cycle.
m_{res}	Trapped residual mass.
m_c	Mass of total charge.
η_m	Combustion efficiency.
c_v	Specific heat for a given composition.
R	Gas constant for a given composition.
q_{lhv}	Heating value of the fuel.
AFR_s	Stoichiometric air–fuel ratio.
EVO/C	Exhaust valve open/close.
IVO/C	Intake valve open/close.
NVO	Negative valve overlap.
ω	Engine speed.
V	Cylinder volume.
θ_x	Crank angle of position x.
$\bar{\theta}_{50}$	Measured crank angle of 50% burned.
$\hat{\theta}_{50}$	Model prediction of θ_{50}.
T	Temperature.
P	Pressure.
λ	Air–fuel ratio.
κ	Adaptive gain.
Θ	Adaptive parameter.
cad	Crank angle degrees.

Manuscript received July 18, 2014; revised December 1, 2014; accepted January 19, 2015. Date of publication March 2, 2015; date of current version October 12, 2015. Manuscript received in final form January 30, 2015. This work was supported in part by the Advanced Research Projects Agency-Energy within the Department of Energy through the National Energy Technology Laboratory under Award DE-EE0003533 and in part by the ACCESS Project consortium, such as Robert Bosch LLC, Farmington Hills, MI, USA, Emitec Inc., Rochester Hills, MI, USA, with direction from H. Yilmaz and O. Miersch-Wiemers, Robert Bosch, LLC, Farmington Hills. Recommended by Associate Editor S. Di Cairano.

J. Larimore, S. Jade, E. Hellström, and A. G. Stefanopoulou are with the Department of Mechanical Engineering, University of Michigan, Ann Arbor, MI 48109 USA (e-mail: larimore@umich.edu; sjade@umich.edu; erikhe@umich.edu; annastef@umich.edu).

L. Jiang is with Robert Bosch LLC, Farmington Hills, MI 48331 USA (e-mail: li.jiang@us.bosch.com).

Color versions of one or more of the figures in this paper are available online at http://ieeexplore.ieee.org.

Digital Object Identifier 10.1109/TCST.2015.2402235

I. INTRODUCTION

HOMOGENEOUS charge compression ignition (HCCI) is a promising combustion strategy that can achieve high thermal efficiency with low engine-out emissions when compared with traditional spark-ignited combustion [1]. It is characterized by compression-driven near-simultaneous autoignition events at multiple sites throughout a homogeneous mixture [2]. Autoignition timing in HCCI combustion requires careful regulation of the temperature, pressure, and composition of the precombustion cylinder charge. This has been accomplished in the previous works by various means, for example, rebreathing in [3], intake air heating in [4] and [5], and dual fuel combustion phasing control in [6]. The control of charge properties in this paper is carried out via recompression HCCI. When using recompression HCCI, a large fraction of the postcombustion residual gases are retained, before they can be exhausted, for the next cycle [7]. This introduces a strong internal feedback mechanism. In addition, the charge properties are regulated through the start of injection (SOI) timing, which is typically realized during the recompression period [8], [9]. This paper presents a method for controlling the combustion phasing of an HCCI engine while adaptively modifying the feedforward controller, developed in [10] and [11], which augmented the midranging feedback controllers in [12] and [13]. An overview of the adaptive control structure is given in Fig. 1.

Model-based control of recompression HCCI requires the development of accurate control-oriented models that can be executed in real time on embedded control hardware. Models have been used to design feedforward and feedback strategies for combustion phasing control in [14] and [15] and for feedback gain selection and gain scheduling in [16]–[19]. Nonlinear feedback using model-based estimation was done in [20] and model-based predictive control strategies were demonstrated in [11] and [21]–[23].

Performance and stability robustness of the closed-loop-controlled HCCI combustion is of great importance, provided

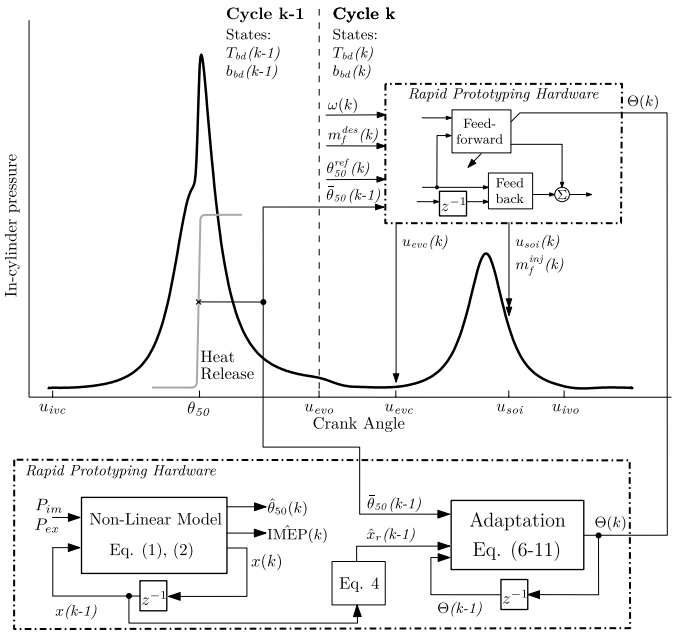

Fig. 1. Graphical representation of the adaptive control structure. Cycle definition, the model inputs, and outputs as well as the states are indicated as well as the basic block diagram of the adaptive parameter estimation and the adaptive parameter changing the feedforward control.

that HCCI combustion can be open loop unstable at various operating conditions, as shown in [24]–[27] and recently in [28] and [29]. The combustion phasing must remain within a narrow acceptable range to satisfy stability and mechanical constraints, as demonstrated in [30] and [31]. However, there are few papers that address control design and adaptation with model uncertainty. For instance, in [32], a method of determining a bilinear parametric model of combustion phasing is applied in simulations for the regulation of combustion phasing in an HCCI engine. Adaptive parameter estimation has also been used in [33] to improve the fidelity of Spark Ignition engine models and for air–fuel ratio control purposes in [34]–[37]. Here, the midranging control structure adapted from [11], [38], and [39] is used to control load transitions with adaptive feedforward, as shown in Fig. 1. Midranging control is a method used primarily in process-control applications [40], [41]; however, it has been utilized successfully in engines for the combustion control where similar coarse and fine trim actuators are often available [13], [42]. To help speed up load transitions and better regulate combustion phasing, the midranging controller is augmented with linear model-based feedforward control. This paper advances this state of the art by introducing adaptive parameter estimation into the feedforward controller of [38] and [39]. This paper addresses, for the first time, potential model mismatch with experimental behavior and helps ensure that the control remains accurate.

Adaptive parameter estimation provides several benefits. First, the adaptation is capable of making adjustments to mitigate modeling errors, as shown in [43]. Second, as will be shown experimentally, a single-model parameterization can be propagated to all four cylinders which reduces model calibration effort. This is beneficial because the current HCCI model requires parameterization, which is nontrivial and time intensive. Furthermore, the adaptive model makes adjustments to the controller throughout the lifetime of the engine, which helps mitigate modeling errors and sensitivity to engine aging and environmental conditions. The adaptive control is implemented on a four-cylinder engine. Experiments are presented that show the comparison between the adaptive and nonadaptive controllers, where an average reduction of 41% in the absolute value of SOI feedback effort at steady state is achieved. In addition, the controller's stability and convergence properties are evaluated through simulations.

This paper is organized as follows. First, the experimental setup is described in Section II followed by an overview of the HCCI model in Section III. The model is then modified in Section IV to include the adaptive parameter estimation scheme, and an analysis of the adaptive parameter's authority on the model output is performed. The controller structure is described in Section VI, and the experimental results are provided in Section VIII. The conclusion is then drawn in Section IX.

II. Experimental Setup

A four-cylinder 2-L General Motors LNF Ecotec engine running research grade gasoline was used as the baseline platform. To accommodate HCCI combustion, the compression ratio was rised to 11.25:1 and camshafts with shorter duration and lower lift were used to allow for unthrottled operation with NVO, which is a method used to retain large amounts of internal residuals. A small supercharger (Eaton M24) was added to the air path in series with the stock turbocharger to provide additional boosting capabilities. The stock turbo charger is too large to generate boost when running HCCI due to the low exhaust enthalpy. The results here were run at approximately 1.1-bar intake manifold pressure, engine speeds of 1600 and 1800 r/min, and loads between 3.0- and 3.8-bar net-indicated mean effective pressure (IMEP), the air–fuel ratio was not controlled; however, it was approximately $\lambda = 1.2$ throughout these tests. The engine coolant temperature was controlled to a set point of 90 °C. The spark was left on, but at a position of 40° after top dead center of combustion. Since the mixture is lean and highly diluted with residuals, the spark will have little influence on the combustion; having the spark on late only helps prevent the spark plugs from fouling.

Cylinder pressures were sampled at a resolution of 0.1° cad for offline pressure analysis; however, real-time estimation of combustion features were done at a resolution of 1° cad. The combustion phasing used in feedback and for the adaptive algorithm was determined with a Bosch Motronic MED 17 engine control unit (ECU). The control strategies were implemented using a combination of C and MATLAB code, and were tested in real time using an ETAS ES910 rapid prototyping module. The ES910 uses an 800-MHz Freescale PowerQUICC III MPC8548 processor with double-precision floating-point arithmetic and 512 MB of RAM.

III. HCCI Model

The discrete time low-order model developed in [10], [11], and [38] is used for control purposes.

The model, modified for online adaptation, consists of two dynamic states used to capture cycle to cycle interactions. They are as follows:

1) T_{bd}: the temperature of the blowdown gases, which is used to represent the recycled thermal energy from one cycle to the next;
2) b_{bd}: the burned gas fraction of the blowdown process, which represents the composition dynamics of each cycle.

The blowdown process is a rapid expansion of exhaust gases during the exhaust stroke, where the pressures of the cylinder and exhaust system equalize quickly. The states are defined immediately after the blowdown process and are given by

$$T_{bd}(k) = T_{\text{ivc}}(k-1)\left(\frac{p_{\text{ivc}}(k-1)}{p_{em}}\right)^{\frac{1-n}{n}} \times\left[1+\frac{\eta_m(k-1)q_{lhv}RV_{50}{}^{n-1}}{c_v\, p_{\text{ivc}}V_{\text{ivc}}{}^{n}}m_f(k-1)\right]^{\frac{1}{n}} \quad (1)$$

$$b_{bd}(k) = \frac{(\text{AFR}_s+1)m_f(k-1)}{m_c(k-1)} + \Theta\hat{x}_r(k-1)b_{bd}(k-1). \quad (2)$$

The value of T_y, V_y, and p_y are the temperature, volume, and pressure at the indicated valve timing. Specifically, the temperature at the time of IVC is given by

$$T_{\text{ivc}}(k-1) = \Theta\hat{x}_r(k-1)T_{\text{res}}(k-1) + (1-\Theta\hat{x}_r(k-1))T_{im} \quad (3)$$

where T_{res} is the residual gas temperature as defined in [10], [11], and [38], T_{im} is the intake manifold temperature, and Θ is the adaptive parameter, which modifies the residual gas fraction x_r, presented in the following sections. When no adaptation is in place, $\Theta = 1$. The residual gas fraction estimate $\hat{x}_r$ is

$$\hat{x}_r(k-1) = 1-(c_0+c_1\theta_{\text{evc}}(k-1))\left(\frac{p_{im}(k-1)}{p_{em}(k-1)}\right)^{c_2} \times T_{bd}(k-1)^{c_3}\omega(k-1)^{c_4} \quad (4)$$

where $c_{0,1,2,3,4}$ are the coefficients tuned to steady-state data, θ_{evc} is the crank angle of EVC, and ω is the engine speed. The values of p_{im} and p_{em} are the intake and exhaust manifold pressures, respectively. The combustion efficiency η_m is defined by a sigmoid in [10], [11], and [38] and is a function of the estimated combustion phasing $\hat{\theta}_{50}$, which is the point at which 50% of the charge has burned. The model depends on several constants: the lower heating value of the fuel q_{lhv}, the gas constant R, polytropic coefficient n, specific heat c_v, and the stoichiometric air–fuel ratio AFR_s. The total charge mass is defined by $m_c = m_{\text{air}} + m_f + m_{\text{res}}$, where m_{air} is the fresh air mass inducted into the cylinder and $m_{\text{res}} = x_r m_c$.

The model has three inputs: 1) the mass of fuel injected (m_f); 2) the SOI timing; and 3) the timing of the EVC. The crank angle difference between the EVC and the IVO is known as the NVO region. The EVC timing controls the amount of NVO, because for these tests, IVO timing was fixed. Varying the amount of NVO directly controls the amount of residuals trapped inside the cylinder. The residual mass has a direct impact on the charge composition and temperature. The model has two outputs, the combustion phasing when 50% of the charge had been burned ($\hat{\theta}_{50}$) and the engine torque denoted by the IMEP.

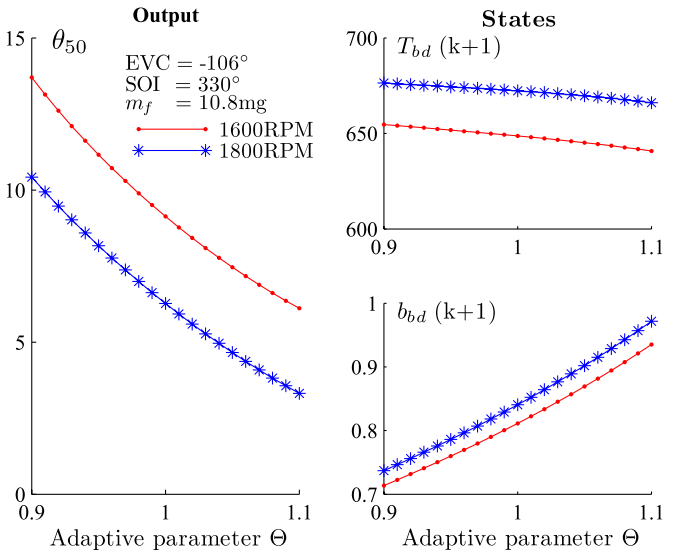

Fig. 2. Sweep of the adaptive parameter Θ shows its effect on the model states T_{bd} and b_{bd} (right) and the model output θ_{50} (left). The effect on θ_{50} is approximately affine.

IV. Parametric Model

The HCCI combustion model in (1) and (2) is nonlinear and requires parameterization, which is nontrivial and time consuming, and it is, therefore, desirable to minimize this effort. In addition, the model is control oriented and is susceptible to modeling errors. One method to reduce parameterization effort and minimize modeling errors is to include adaptive parameters. The selection of an adaptive parameter or parameters is challenging due to the model's nonlinearities. Ideally, one would want to achieve a large authority over the model's output with a small number of physically sensible adaptive parameters. Since the combustion phasing in HCCI is most significantly influenced by T_{ivc} and the value of T_{ivc}, as shown in (3), has a high sensitivity to the modeled residual gas fraction x_r, it was concluded that the adaptive parameter would scale the model's estimate of the residual gas fraction $\Theta\hat{x}_r$. Placing the adaptive parameter on the residual gas fraction, rather than T_{ivc}, allows for the formation of a linear parametric model and the use of a simple parameter estimation law. In addition, the placement of the adaptive parameter on the residual gas fraction results in strong effect on the model output (θ_{50}), as shown in Fig. 2. It is recognized that not all errors, such as unmodeled thermal dynamics or heat transfer, should be attributed to this term. However, since many of these sources of model error are relatively unknown, all errors are lumped into the residual gas fraction in the simplified control-oriented model.

To determine the parameter Θ, an error term is required

$$\epsilon(k-1) = \bar{x}_r(k-1) - \Theta(k-1)\hat{x}_r(k-1) \quad (5)$$

where $\bar{x}_r$ would ideally be the measured value of the residual gas fraction x_r. It is, however, extremely difficult to measure the residual gas fraction of an engine, especially on board a vehicle. We therefore employ the measurement of the combustion phasing $\bar{\theta}_{50}$, computed by the ECU through the use of the in-cylinder pressure sensors and online heat release analysis.

The data suggest that the combustion phasing model can be well approximated by the quadratic expression

$$\bar{\theta}_{50}(k-1) = \alpha_{\theta 1} T_{\text{ivc}}^2(k-1) + \alpha_{\theta 2} T_{\text{ivc}}(k-1) + \alpha_{\theta 3} \tag{6}$$

where $\alpha_{\theta 1,2,3}$ are the functions of the injection timing. This approximation has been validated extensively with experiments on a multicylinder engine across a broad range of operating conditions. Through inversion of this model, the value of T_{ivc}, which was necessary for the measured combustion phasing ($\bar{T}_{\text{ivc}}$) of the previous cycle, is given by

$$\bar{T}_{\text{ivc}}(k-1) = \frac{-\alpha_{\theta 2} - \sqrt{\alpha_{\theta 2}^2 - 4\alpha_{\theta 1}(\alpha_{\theta 3} - \bar{\theta}_{50}(k-1))}}{2\alpha_{\theta 1}}. \tag{7}$$

The other solution to (6) is always a nonphysical solution, since $\alpha_{\theta 1}$ is negative. The result obtained by (7) is dependent on the measurement of combustion phasing and is therefore more accurate than the result obtained by the model's regression. If we then employ a mass balance at IVC as shown in

$$\bar{T}_{\text{ivc}}(k-1) = \bar{x}_r(k-1) T_{\text{res}}(k-1) + (1 - \bar{x}_r(k-1)) T_{im} \tag{8}$$

where T_{im} is the measured intake manifold temperature and T_{res} is the residual gas temperature given by the model in [10], then the value of $\bar{x}_r$ is simply

$$\bar{x}_r(k-1) = \frac{\bar{T}_{\text{ivc}}(k-1) - T_{im}}{T_{\text{res}}(k-1) - T_{im}}. \tag{9}$$

By developing a parametric model of this form, linear parameter estimation laws can be applied.

V. Adaptive Law

The discrete gradient parameter estimation law given in (10) is used to determine the value of Θ based on online measurements for each cycle. This enables the model adaptation. The equation and its stability properties are derived in [44] for linear systems. The speed at which the algorithm converges is controlled by the constant gain κ. It is important that the gain is tuned to enforce slow convergence and has a minimal impact on the transient response of the system. The rate of convergence of the adaptive parameter will be addressed in greater detail in Section V-B

$$\Theta(k) = \frac{\kappa \bar{x}_r(k-1)\epsilon(k-1)}{\bar{x}_r(k-1)^2 + c_\Theta} + \Theta(k-1) \quad \text{where} \quad \kappa, c_\Theta = \text{constants}. \tag{10}$$

There are two conditions to avoid with this formulation: $\bar{x}_r^2 + c_\Theta = 0$ and $\bar{x}_r\epsilon, \bar{x}_r^2 + c_\Theta \to \infty$. Division by zero is prevented because c_Θ is small and positive, and additionally, and since $\bar{x}_r \in [0, 1]$, the denominator will remain positive and cannot grow unboundedly. The value of $\bar{x}_r\epsilon$ will stay bounded provided the error ϵ is bounded. To avoid unwanted behavior however, the value of Θ is also restricted, through the saturation of the output, to be within $\Theta \in [0.9,\ 1.2]$. It is unlikely that the actual in-cylinder residual gas fraction changes by more than 10%–20% over short periods of time for this system. There are many ways to mitigate unwanted parameter drift [45].

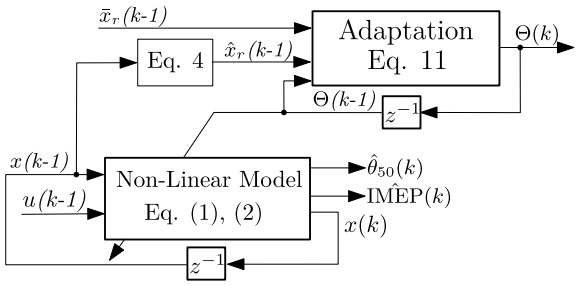

Fig. 3. Simplified system used for analyzing the stability of the estimation scheme. The value of $\bar{x}_r$ is treated as an input to the system. Note that the stability of the adaptive controller in Fig. 1, when the estimator is used for the adaptation of $\bar{x}_r$, is analyzed in Section VII.

A. Authority of Adaptive Parameter

To observe the effect that the adaptive parameter has on the system, simulations were performed for the range of possible Θ values. At each point, the model was allowed to come to steady state and the values of T_{bd}, b_{bd}, and the predicted combustion phasing were observed (Fig. 2). The sweep was performed at both 1800 and 1600 r/min. This simulation and the linearization in Section V-B were done with 10.8 mg of fuel, an SOI of 330° before TDC of combustion, and an EVC of −106° after TDC of gas exchange. The adaptive parameter has an approximately affine effect on the model output with relatively high sensitivity. This indicates that the adaptive parameter selection is well suited for the control objective.

B. Stability

To evaluate the stability of the adaptive parameter estimation scheme, the simplified system in Fig. 3 is analyzed. Here, the estimated residual gas fraction from a measurement of combustion phasing, $\bar{x}_r$, is treated as an input to the system. A state update equation for Θ can then be derived by combining (5) and (10) to get

$$\Theta(k) = \frac{\kappa \bar{x}_r^2(k-1)}{\bar{x}_r^2(k-1) + c_\Theta} + \Theta(k-1)\left(1 - \frac{\kappa \bar{x}_r(k-1)\hat{x}_r(k-1)}{\bar{x}_r^2(k-1) + c_\Theta}\right). \tag{11}$$

To investigate the stability of the adaptive parameter estimation, we must demonstrate that at steady state, Θ converges to a value that causes the error ϵ in (5) to go to zero. Let us define with * the equilibrium values for which $\epsilon = 0$. If we solve (5) for Θ when $\epsilon = 0$, we can see that $\Theta^* = \bar{x}_r^*/\hat{x}_r^*$. Equation (11) is linearized about the steady-state parameter value (Θ^*) as well as the steady-state values of the states T_{bd} and b_{bd} in (1) and (2). The linear system is obtained

by substituting (4) into (11) and then analytically linearizing the result around the stationary operating point $(\Theta^*, T_{bd}^*, \bar{x}_r^*)$

$$\begin{aligned}\Delta\Theta(k) = &\left(1 - \frac{\kappa \bar{x}_r^* \hat{x}_r^*}{\bar{x}_r^{*2} + c_\Theta}\right)\Delta\Theta(k-1) \\ &+ \left(\frac{\kappa \alpha c_3 \bar{x}_r^{*2} T_{bd}^{*(c_3-1)}}{\hat{x}_r^*(\bar{x}_r^{*2} + c_\Theta)}\right)\Delta T_{bd}(k-1) \\ &+ \left(\frac{\kappa \bar{x}_r^*}{\bar{x}_r^{*2} + c_\Theta}\right)\Delta \bar{x}_r(k-1) \end{aligned} \tag{12}$$

where

$$\alpha = \Pi^{c_2}(c_0 + c_1\theta_{\text{evc}})\omega^{c_4}, \quad \Pi = \frac{p_{im}}{p_{em}}.$$

This equation can be augmented with a linearization of the system in (1) and (2), where Θ is added as a multiplicative modification to the residual gas fraction. This is the system represented in Fig. 3. The linearization was achieved numerically using MATLAB Simulink to yield

$$\begin{bmatrix} \Delta T_{bd}(k) \\ \Delta b_{bd}(k) \\ \Delta\Theta(k) \end{bmatrix} = \begin{bmatrix} 0.4871 & -93.2017 & 84.1512 \\ -0.0001 & 0.5176 & 0.5494 \\ \left(\frac{\kappa \alpha c_3 \bar{x}_r^{*2} T_{bd}^{*(c_3-1)}}{\hat{x}_r^*(\bar{x}_r^{*2} + c_\Theta)}\right) & 0 & \left(1 - \frac{\kappa \bar{x}_r^* \hat{x}_r^*}{\bar{x}_r^{*2} + c_\Theta}\right) \end{bmatrix} \cdot \begin{bmatrix} \Delta T_{bd}(k-1) \\ \Delta b_{bd}(k-1) \\ \Delta\Theta(k-1) \end{bmatrix} + \begin{bmatrix} B_{11} & 0 \\ B_{21} & 0 \\ 0 & \left(\frac{\kappa \bar{x}_r^*}{\bar{x}_r^{*2} + c_\Theta}\right) \end{bmatrix} \begin{bmatrix} \Delta u_{ss}(k-1) \\ \Delta \bar{x}_r(k-1) \end{bmatrix} \tag{13}$$

where

$$\begin{aligned} B_{11} &= [-1.6, 33.2, -0.02, 0.08] \\ B_{21} &= [-0.004, 0.04, 0, 0] \\ \Delta u_{ss} &= \left[u_{\text{evc}}^*, m_f^*, u_{\text{soi}}^*, \omega^*\right]. \end{aligned}$$

This augmented system allows us to observe the effect the adaptive parameter has on the dynamics of the temperature and composition states as well as the eigenvalue of the adaptive parameter state itself. This is shown through the root locus plot of Fig. 4. Here, we can see that when the adaptive gain κ is 0, the eigenvalues of the temperature and composition dynamics are the same as those of the system with no adaptation, in which both are on the positive real axis. In addition, the eigenvalue of Θ is one. As κ is increased, the eigenvalues of the system approach each other and eventually break off into the imaginary plane. At approximately $\kappa = 1$, the system becomes unstable. The eigenvalue associated with the adaptive parameter is pulled in while κ increases indicating that the parameter will converge faster with a higher gain, as is expected. For small gains, the system is stable, which indicates that ϵ will converge to 0.

To demonstrate how the adaptive parameter converges, the system in Fig. 3, as summarized by (13), was simulated with a value of $\bar{x}_r$ and constant inputs u that corresponded to $\Theta^* = 0.9$ and $\bar{\theta}_{50} = 8.2$. Three different adaptive gains were tested. The simulation results are shown in Fig. 5 and it can be observed that the system successfully converges to the unknown parameter Θ^* and the desired combustion phasing $\bar{\theta}_{50}$. A gain of $\kappa = 0.005$ was used for the tests presented in the following sections, because it offers good convergence response without pulling off the temperature and composition eigenvalues of the real axis.

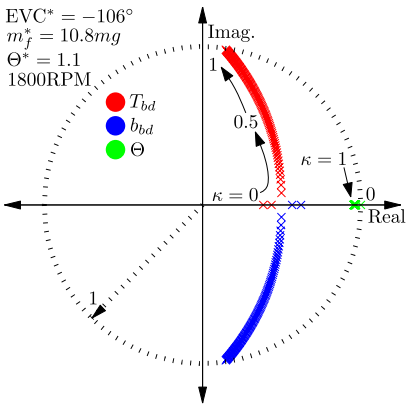

Fig. 4. Root locus of the eigenvalues associated with the system in (13). As κ is increased, the adaptation occurs more quickly, but the underlying system eventually becomes unstable.

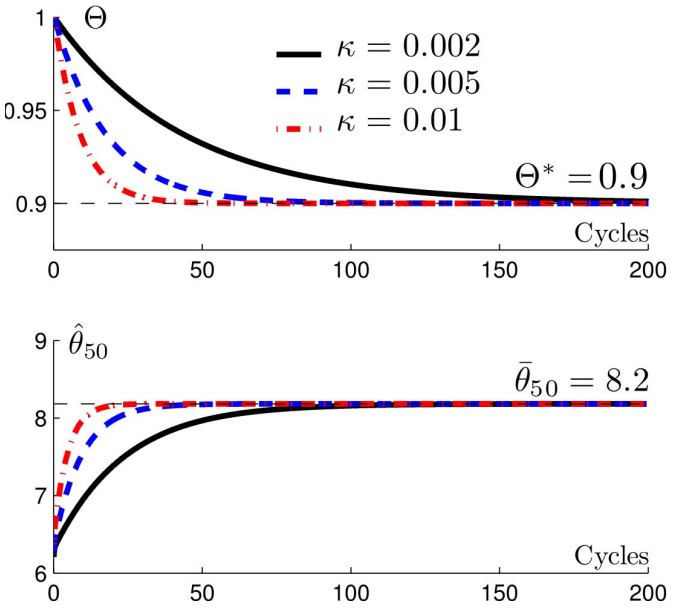

Fig. 5. Convergence of the adaptive parameter to a set point with different gains through the simulations of the system in Fig. 3, the prediction of combustion phasing $\hat{\theta}_{50}$ also converges to the measured combustion phasing $\bar{\theta}_{50}$.

VI. Controller

The midranging controller with the linear feedforward developed in [10] and [11] is used here as a baseline controller for the regulation of combustion phasing (θ_{50}). The regulation of combustion phasing in an HCCI engine is critical due to its sensitivity to cyclic variability at late combustion phasing and the excessive pressure rise rates for early θ_{50}. As such, the controller objective is to regulate θ_{50} to a desired reference

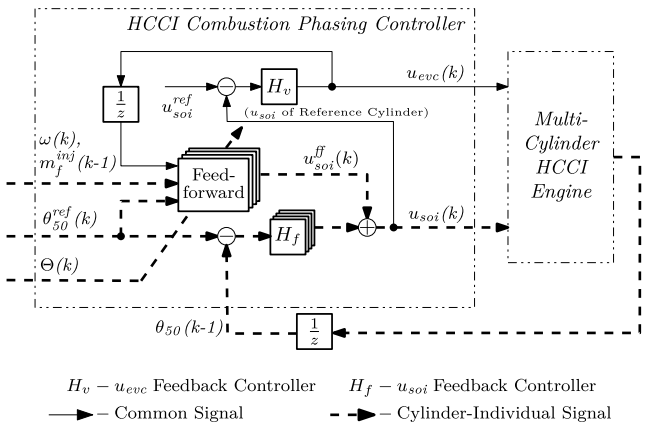

Fig. 6. Midranging control architecture for a multicylinder engine. Here, the coarse and fine trim actuators are u_{evc} and u_{soi}, respectively [10].

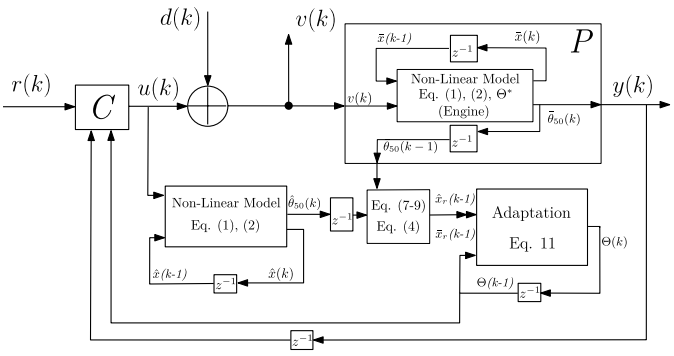

Fig. 7. Block diagram of the complete system as implemented for the simulation of the small signal stability analysis. The engine is replaced by a linearized model.

set point during load transitions. This set point is typically determined offline or provided by a supervisory controller.

The baseline controller uses the u_{evc} and u_{soi} actuators to regulate θ_{50} in a midranging configuration, where the coarse and fine actuators are u_{evc} and u_{soi}, respectively. This architecture is demonstrated graphically in Fig. 6, which has been adapted from [10]. The u_{evc} actuator has a large range and high authority. However, since the hydraulic cam phasers are slow and there is a single intake and exhaust camshaft for all four cylinders, a single value of EVC must be applied for all cylinders. The u_{soi} actuator can be changed on a cycle-by-cycle and cylinder-by-cylinder basis, however, its authority is small, and it can saturate quickly depending on the operating condition. Therefore, the actuator u_{evc} strives to midrange u_{soi} back to a set point that is chosen to be in its region of greatest authority. The θ_{50} tracking error signal drives the controller for u_{soi}. This midranging control structure has been used successfully to navigate transients in various actuators including throughout a large load and speed operating region in [11]. Using the adaptive scheme, we can mitigate errors and adjust the SOI control based on the adaptation of Θ and the θ_{50} tracking error.

The feedforward component of u_{soi} from [10] is modified here to incorporate the adaptive parameter, which is taken as an input. The feedforward control is found by linearizing the nonlinear model summarized by (1) and (2) about a typical HCCI operating point. Specifically, $u_{\text{evc}} = -106°$ aTDC, SOI $= 330°$ bTDC, $m_f = 10.8$ mg, and an engine speed of 1800 r/min are used. The linearized model inverted at steady state is

$$\begin{aligned} x_{ss} &= Ax_{ss} + B_{\text{soi}}u_{\text{soi}}^{ff} + B_{\text{evc}}u_{\text{evc}} + B_f m_f^{inj} + B_\omega \omega + B_\Theta \Theta \\ \theta_{50}^{\text{ref}} &= Cx_{ss} + D_{\text{soi}}u_{\text{soi}}^{ff} + D_{\text{evc}}u_{\text{evc}} + D_f m_f^{inj} + D_\omega \omega + D_\Theta \Theta \\ \therefore u_{\text{soi}}^{ff} &= \begin{bmatrix} 0 \\ 1 \end{bmatrix}^T \begin{bmatrix} (A-I) & B_{\text{soi}} \\ C & D_{\text{soi}} \end{bmatrix}^{-1} \begin{bmatrix} -B & 0 \\ -D & 1 \end{bmatrix} \\ &\quad \times \begin{bmatrix} u_{\text{evc}}, & m_f^{inj}, & \omega, & \Theta, & \theta_{50}^{\text{ref}} \end{bmatrix}^T \end{aligned} \tag{14}$$

where

$$B = \begin{bmatrix} B_{\text{evc}} & B_f & B_\omega & B_\Theta \end{bmatrix}$$
$$D = \begin{bmatrix} D_{\text{evc}} & D_f & D_\omega & D_\Theta \end{bmatrix}.$$

The feedforward injection timing u_{soi}^{ff} is the timing necessary for a given reference combustion phasing, assuming all other inputs are at steady state. The reference combustion phasing was set to 8.5° aTDC for these tests. It can also be seen that the equations have been appropriately modified to incorporate the adaptive gain Θ that presents itself in the B and D matrices. The feedforward block is then a fixed gain for a given cycle. Since each cylinder can have a different fuel mass and combustion phasing reference and because u_{evc}, ω, and Θ are constantly varying parameters, the controller computes a gain for each cylinder on each cycle. The eigenvalues for this system are real and lie on the positive axis, they are less than one and are therefore stable. For significantly later values of u_{evc}, the model predicts the onset of high cyclic variability in the form of oscillatory dynamics [11].

The value of Θ pushes the steady-state value of the states closer to that of the actual engine based on the measured combustion phasing, as presented in Section IV. This in turn yields a control u_{soi}, which is more accurate.

A graphical representation of the complete system is provided in Fig. 1. Here, it can be seen how the continuous-time system is separated into discrete cycles, where the measurements are taken and where inputs are applied. The adaptive algorithm and nonlinear model run alongside the midranging controller on the rapid prototyping hardware.

VII. Closed-Loop Stability

The system of Fig. 1 can be represented in simulation by the block diagram of Fig. 7, where the engine is replaced by a linearized model and the controller is as described in the preceding sections. The closed-loop transfer function from input to output [$r(k)$ to $y(k)$] has poles at $\{0.997,\ 0.970,\ 0.855, 0.664, 0.622, 0.383, 0.250,\ -0.001\}$, which all lie within the unit circle and are therefore locally stable. The poles which are close to 1 correspond to the adaptive state and integrators in the controllers. These integrators are being pulled away from 1 by the adaptive gain and

closed-loop zeros. The following stability analysis is linear and therefore local as well.

To analyze the internal stability of the system, the four-transfer-function matrix theorem [46] is applied from the inputs r and d to the outputs y and v, as indicated in Fig. 7. Here, the reference signal r is the desired combustion phasing and the output y is the measured combustion phasing. The values of d is a disturbance and the value of v is the disturbance plus the control actuation. The system is given by

$$\begin{bmatrix} Y \\ V \end{bmatrix} = T_{4TF} \begin{bmatrix} R \\ D \end{bmatrix} \tag{15}$$

where Y, V, R, and D are the z-transform representation of the y, v, r, and d signals, respectively. The four transfer functions can be summarized by

$$T_{4TF} = \begin{bmatrix} T_O & PS_I \\ S_I C & S_I \end{bmatrix} \tag{16}$$

where T_O is the output complementary sensitivity function (from r to y) and S_I is the input sensitivity function (from d to v). The plant and controller are P and C, respectively, and the plant has poles at $\{0.38\ 0.62\}$. Since the plant and controller have no unstable poles and all poles of the four transfer functions in T_{4TF} are also stable, the four transfer function theorem for multivariable systems indicates that the closed-loop system is internally stable.

VIII. Experimental Results

The adaptive controller was implemented in real time on the experimental setup from Section II. The model inverted for feedforward control was parameterized with data from one cylinder and then duplicated for the remaining three. Cylinder-to-cylinder variations are large enough to warrant the cylinder individual parameterizations; however, it will be shown through steady-state tests that the adaptive controller alleviates this need. In addition, transient tests will show the controller's ability to perform load steps and correct for the modeling errors before and after transitions.

A. Feedback Effort Reduction

To demonstrate the adaptive controller's ability to correct for modeling errors and uncertainty, a test was run in which the engine was allowed to come to a steady state with the baseline controller active, at which point the adaptive gain was applied to the feedforward control. For this test, the combustion phasing is regulated to its reference position and does not move much, with the exception of typical cycle-to-cycle variability. The test was run as close to the linearization point as possible; however, there are clear cylinder-to-cylinder variations. The effect on the feedforward control can be found in Fig. 8. The adaptive algorithm is turned on at $t = 20$ s, at which point the adaptive gain pushes the feedforward part of the control closer to the set point of 330°, indicating that the model is more correctly representing the physical system. In addition, the total SOI (feedforward plus feedback) remains the same for both the adaptive and nonadaptive.

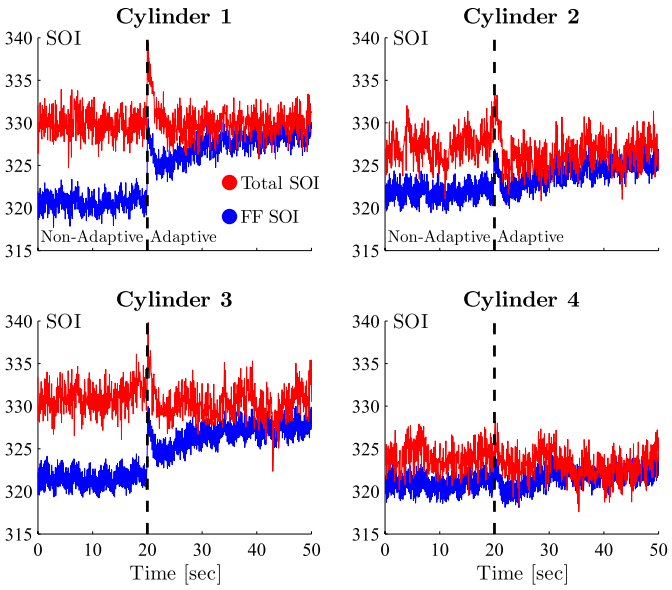

Fig. 8. Adaptive control makes the model-based feedforward control more accurate when activated at 20 s. The result is similar for all four cylinders even though they all are at slightly different operating conditions and have the same parameterization.

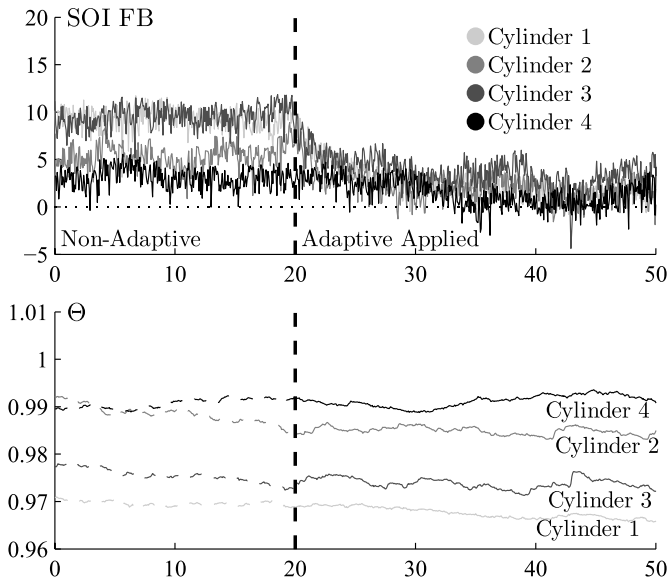

Fig. 9. Feedback control is minimized by the adaptive gain making the feedforward control more accurate, as shown in Fig. 8. In addition, the adaptive parameter Θ is shown to go to different values for each cylinder.

The effect on the feedforward SOI is further shown in Fig. 9, where the feedback effort is observed. It is clear here that the feedback effort after the adaptive parameter is activated is reduced and that it tends toward zero. The amount by which the adaptive gain Θ must modify the model inversion is shown in the second plot of Fig. 9. The difference in Θ for the four cylinders indicates that the model's parameterization for some cylinders was better than for others, and the deviation from unity indicates more correction by the adaptive parameter. This also indicates that the adaptive parameter has effectively made corrections to each cylinder's model parameterization

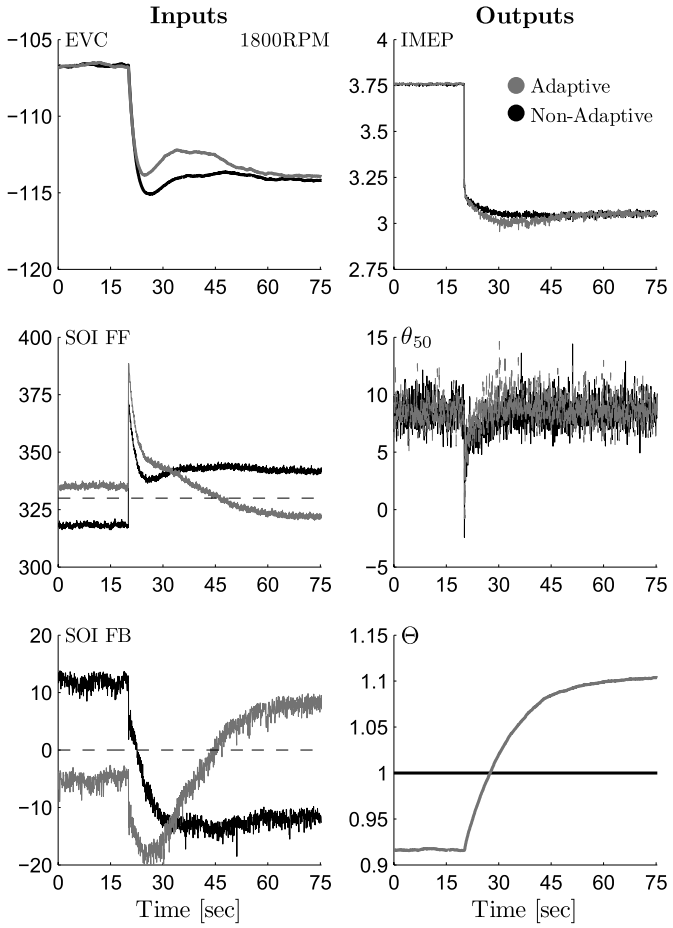

Fig. 10. Load step from 3.75- to 3-bar IMEP at 1800 r/min. Feedforward is more accurate with adaptive control, and the transient effort required by EVC is reduced.

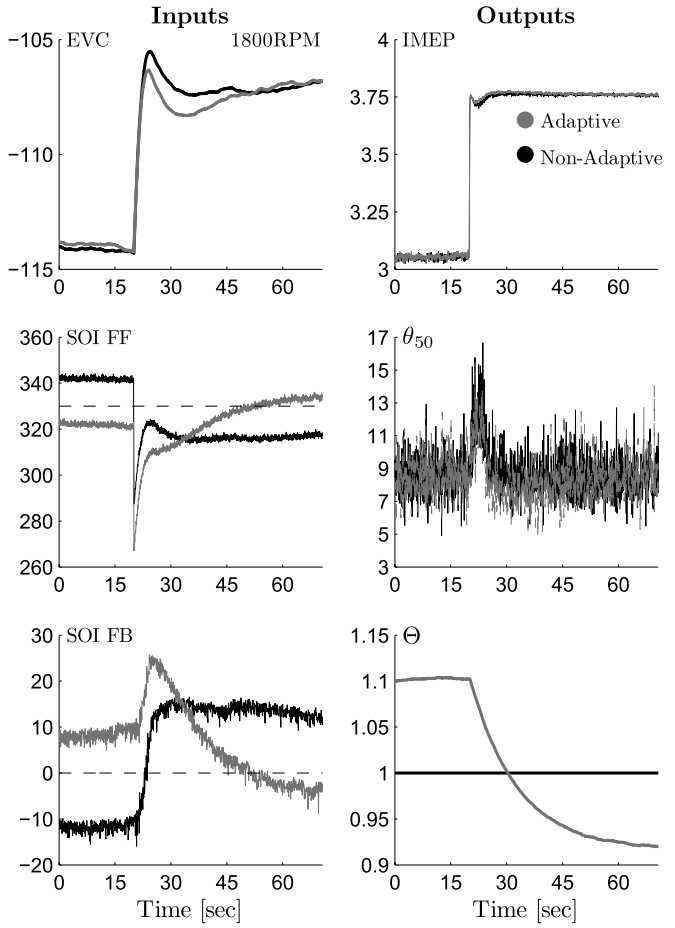

Fig. 11. Load step from 3- to 3.75-bar IMEP at 1800 r/min. Feedforward is more accurate with adaptive control, and the transient effort required by EVC is reduced.

as necessary. Here, the adaptation had already been turned on and converged at the beginning of the test; however, the gain is only applied when indicated. While the gain is applied instantaneously, the control moves slowly because it depends on the slow EVC actuator.

B. Load Steps

Since the feedforward controller is derived via a linear approximation around a specific operating point, the deviation from the linearization point can cause errors in the feedforward component of the control. Even if gain scheduling of the linear controllers or a nonlinear inversion is applied, a slow online correction of the nonlinear model and control will be beneficial. In this section, we demonstrate the benefits of the adaptation in the linearized feedforward control structure through the mitigation of model mismatch. It is the objective of the adaptive controller to mitigate these errors in the steady state. To explore this effect, fuel steps (load steps) were performed in closed loop with and without the adaptive controller active. The adaptive controller was designed to be slow, since it is not the objective of the adaptive parameter to change the transient response of the system but rather adjust the feedforward model inversion to correct for model mismatch or engine aging. This is done so that the feedforward control remains accurate from one set point to the next, but the model's physical basis is relied upon to yield good control during the fast transitions. The result of a load step down from 3.75- to 3-bar IMEP is found in Fig. 10, and this is the result for cylinder 1. Here, we can see that as the load is reduced, the exhaust valve is advanced to trap more residuals and compensate for the drop in temperature associated with the lower load. However, the exhaust valve phases slowly and so during the transition, the SOI is advanced rapidly to allow more time for fuel reformation and advances the combustion. The transient response with and without the adaptation active is comparable in terms of both torque output and regulation of combustion phasing. However, it can be seen that the controller's feedback effort has been reduced at steady state and because of this, the EVC control does less work during the transient. The adaptive parameter is also shown for this load step, where it is clear that the model is incorrectly estimating the residual gas fraction when not using the adaptive model.

Similarly, a load step up is observed in Fig. 11, where the adaptive control provides a similar result. It should also be noted that for both load steps, the adaptive parameter stays within the region where the effect on the system is approximately linear. In an ideal scenario, the adaptive parameter should push the feedback control component to zero;

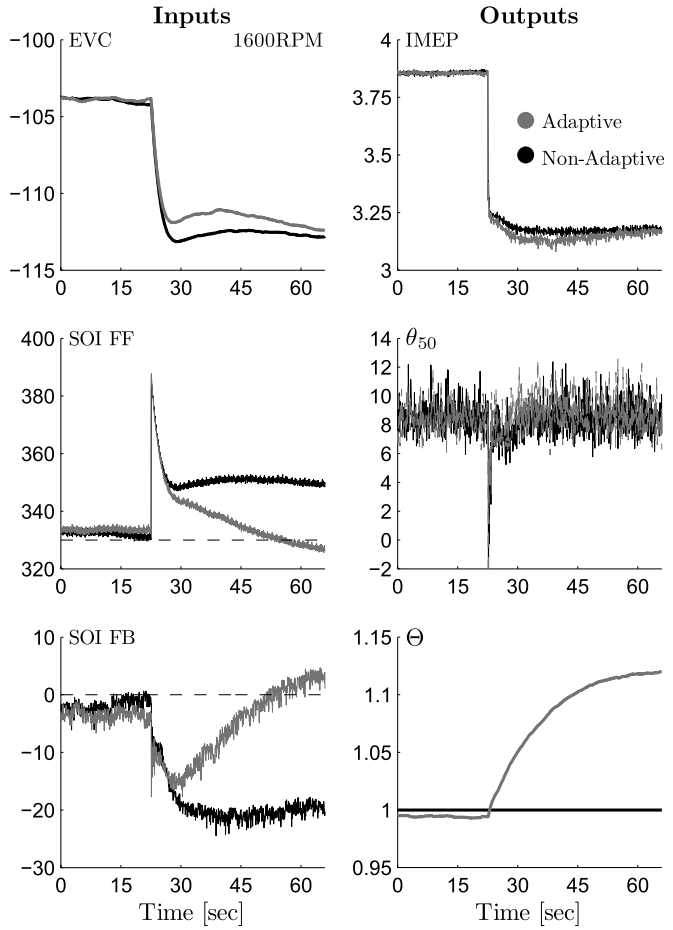

Fig. 12. Load step from 3.8- to 3.25-bar IMEP at 1600 r/min. A significant improvement in the feedforward component of SOI control is observed at 3.25 bar. The transient effort of EVC is also reduced during the transition. The feedforward is accurate at 3.8 bar and the adaptive parameter Θ is close to 1.

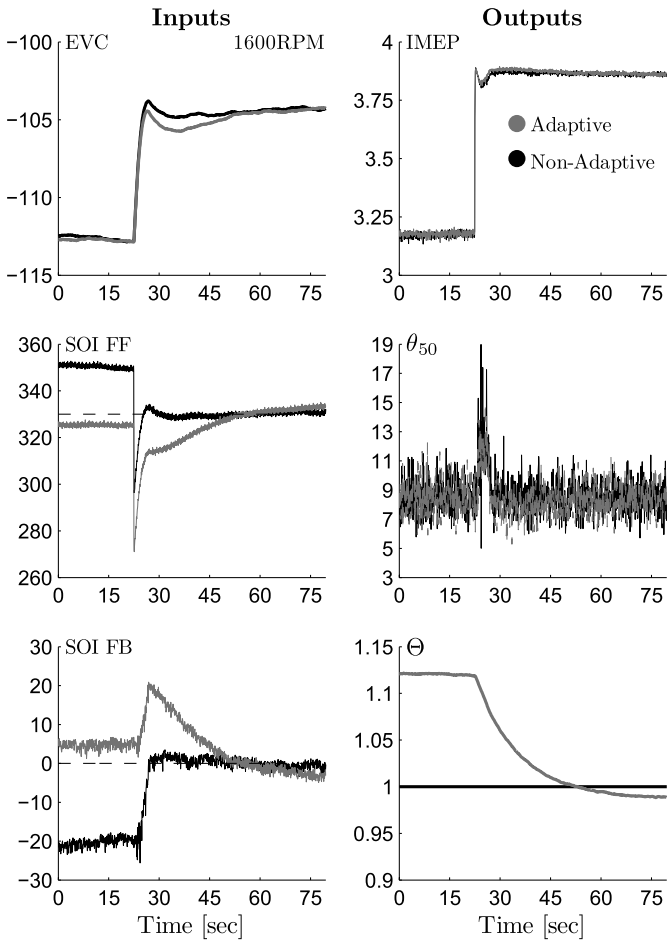

Fig. 13. Load step from 3.8- to 3.25-bar IMEP at 1600 r/min. A significant improvement in the feedforward component of SOI control is seen at 3.25 bar. The transient effort of EVC is also reduced during the transition. The feedforward is accurate at 3.8 bar and the adaptive parameter Θ is close to 1.

however, small changes to the system, such as the temperature and pressure of the intake manifold, can cause errors. The adaptation tries to lump various sources of model mismatch and hence cannot completely eliminate, or replace, the feedback correction.

C. Speed Variation

To quantify the controller's performance away from the linearization point, similar load steps to those of Section VIII-B were run at 1600 r/min, and a load step down is shown in Fig. 12. The feedforward controller has knowledge that the speed has changed to 1600 r/min and the model inversion is accurate at approximately 3.8-bar IMEP. Specifically, the feedfoward SOI is close to the set point and Θ is close to unity. However, when the load is stepped down to 3.25 bar, the feedforward at steady state is very far from the set point and the slow EVC controller is required to do more work. This is despite the fact that engine speed enters into the inversion of the model in the B matrix of (14). When the same transition is made with the adaptive control active, the SOI feedforward quickly returns to the set point and the feedback tends to zero resulting in less EVC effort during the transition. A load step up in Fig. 13 shows similar behavior, and the feedforward controller's performance is improved at 3.25 bar.

TABLE I
STEADY-STATE SOI FEEDBACK EFFORT BEFORE AND AFTER LOAD STEPS. RESULTS SHOWN AS NONADAPTIVE/ADAPTIVE IN CRANK ANGLE DEGREES

	1800RPM		**1600RPM**	
Step	Down	Up	Down	Up
Before	$^{11.82}/_{\mathbf{-5.27}}$	$^{-11.85}/_{\mathbf{7.83}}$	$^{-2.48}/_{\mathbf{-3.24}}$	$^{-17.92}/_{\mathbf{5.07}}$
After	$^{-11.59}/_{\mathbf{8.06}}$	$^{12.26}/_{\mathbf{-3.72}}$	$^{-19.50}/_{\mathbf{2.70}}$	$^{-3.12}/_{\mathbf{-2.79}}$

D. Summary of Results

Table I presents a quantitative summary of the adaptive control results through the absolute value of the steady-state feedback SOI. Specifically, it can be seen that the feedback effort required for nearly all tests is significantly reduced when using the adaptive control. The exception is before the load step down at 1600 r/min; however, at this point,

the feedforward control is already very good without adaptation and so there is little room for improvement. Over all the tests, the average reduction in the absolute value SOI feedback at steady state was 41%.

IX. Conclusion

An adaptive control scheme has been developed and evaluated through the simulations and experiments. The use of an adaptive parameter in the feedforward control helps to improve the accuracy of the controller at steady state. An average reduction in steady-state SOI feedback effort of 41% was achieved. This allows the system to make transitions using mostly feedforward control, which reduces the effort required by the slow EVC actuator. This is particularly useful when using linear model inversion, because any transition will deviate from the linearization point.

In addition, a stability analysis has been performed for both the adaptive parameter estimation scheme and the full closed loop system. It has been shown that the adaptive state is stable for small gains and that the closed loop system is internally stable for typical engine operating conditions. Future work includes extending the feedforward controller to a nonlinear model inversion and using adaptive parameter estimation to further improve the control for the onset of cyclic variability in load transitions. Nonlinear stability analysis could also be a focus of the future work and the use of an adaptive parameter on other physical components of the model could be explored, for instance, heat transfer could be adapted to compensate for slow dynamical changes.

Acknowledgment

The authors would like to thank J. Sterniak and J. Vanier for their help with the experimental hardware and software.

References

[1] M. Yao, Z. Zheng, and H. Liu, "Progress and recent trends in homogeneous charge compression ignition (HCCI) engines," *Prog. Energy Combustion Sci.*, vol. 35, no. 5, pp. 398–437, Oct. 2009.

[2] J. Willand, R. Nieberding, G. Vent, and C. Enderle, "The knocking syndrome—Its cure and its potential," SAE Tech. Papers 982483, 1998.

[3] D. J. Rausen, A. G. Stefanopoulou, J.-M. Kang, J. A. Eng, and T.-W. Kuo, "A mean-value model for control of homogeneous charge compression ignition (HCCI) engines," *J. Dyn. Sys., Meas., Control*, vol. 127, no. 3, pp. 355–362, 2005.

[4] A. Widd, P. Tunestål, and R. Johansson, "Physical modeling and control of homogeneous charge compression ignition (HCCI) engines," in *Proc. 47th IEEE Conf. Decision Control*, Dec. 2008, pp. 5615–5620.

[5] A. Widd, K. Ekholm, P. Tunestål, and R. Johansson, "Physics-based model predictive control of HCCI combustion phasing using fast thermal management and VVA," *IEEE Trans. Control Syst. Technol.*, vol. 20, no. 3, pp. 688–699, May 2012.

[6] J.-O. Olsson, P. Tunestål, and B. Johansson, "Closed-loop control of an HCCI engine," SAE Tech. Paper 2001-01-1031, 2001.

[7] M. J. Roelle, A. F. Jungkunz, N. Ravi, and J. C. Gerdes, "A dynamic model of recompression HCCI combustion including cylinder wall temperature," in *Proc. IMECE*, 2006, pp. 415–424, paper IMECE2006-15125.

[8] N. Wermuth, H. Yun, and P. Najt, "Enhancing light load HCCI combustion in a direct injection gasoline engine by fuel reforming during recompression," *SAE Int. J. Engines*, vol. 2, no. 1, pp. 823–836, 2009.

[9] C. D. Marriott and R. D. Reitz, "Experimental investigation of direct injection-gasoline for premixed compression ignited combustion phasing control," SAE Tech. Paper 2002-01-0418, 2002.

[10] S. Jade, E. Hellström, J. Larimore, A. G. Stefanopoulou, and L. Jiang, "Reference governor for load control in a multicylinder recompression HCCI engine," *IEEE Trans. Control Syst. Technol.*, vol. 22, no. 4, pp. 1408–1421, Jul. 2014.

[11] S. Jade, J. Larimore, E. Hellström, L. Jiang, and A. G. Stefanopoulou, "Enabling large load transitions on multicylinder recompression HCCI engines using fuel governors," in *Proc. Amer. Control Conf.*, Washington, DC, USA, Jun. 2013, pp. 4423–4428.

[12] N. Ravi, H.-H. Liao, A. F. Jungkunz, C.-F. Chang, H. H. Song, and J. C. Gerdes, "Modeling and control of an exhaust recompression HCCI engine using split injection," *J. Dyn. Syst., Meas., Control*, vol. 134, no. 1, pp. 011016-1–011016-12, 2012.

[13] N. Ravi, H.-H. Liao, A. Jungkunz, and J. C. Gerdes, "Mid-ranging control of a multi-cylinder HCCI engine using split fuel injection and valve timings," in *Proc. 6th IFAC*, 2010, pp. 797–802.

[14] G. M. Shaver and J. C. Gerdes, "Cycle-to-cycle control of HCCI engines," in *Proc. ASME Int. Mech. Eng. Congr. Expo.*, 2003, pp. 403–412, paper IMECE2003-41966.

[15] C. J. Chiang and A. G. Stefanopoulou, "Control of thermal ignition in gasoline engines," in *Proc. Amer. Control Conf.*, Jun. 2005, pp. 3847–3852.

[16] G. M. Shaver, J. C. Gerdes, and M. Roelle, "Physics-based closed-loop control of phasing, peak pressure and work output in HCCI engines utilizing variable valve actuation," in *Proc. Amer. Control Conf.*, Jun./Jul. 2004, pp. 150–155.

[17] D. Blom, M. Karlsson, K. Ekholm, P. Tunestål, and R. Johansson, "HCCI engine modeling and control using conservation principles," SAE Tech. Paper 2008-01-0789, 2008.

[18] N. Ravi *et al.*, "Model-based control of HCCI engines using exhaust recompression," *IEEE Trans. Control Syst. Technol.*, vol. 18, no. 6, pp. 1289–1302, Nov. 2010.

[19] G. M. Shaver *et al.*, "A physics-based approach to the control of homogeneous charge compression ignition engines with variable valve actuation," *Int. J. Engine Res.*, vol. 6, no. 4, pp. 361–375, 2005.

[20] C.-J. Chiang, A. G. Stefanopoulou, and M. Jankovic, "Nonlinear observer-based control of load transitions in homogeneous charge compression ignition engines," *IEEE Trans. Control Syst. Technol.*, vol. 15, no. 3, pp. 438–448, May 2007.

[21] J. Bengtsson, P. Strandh, R. Johansson, P. Tunestål, and B. Johansson, "Model predictive control of homogeneous charge compression ignition (HCCI) engine dynamics," in *Proc. IEEE Int. Conf. Control Appl., Comput. Aided Control Syst. Design*, Oct. 2006, pp. 1675–1680.

[22] C.-J. Chiang and C.-L. Chen, "Constrained control of homogeneous charge compression ignition (HCCI) engines," in *Proc. 5th IEEE Conf. Ind. Electron. Appl.*, Jun. 2010, pp. 2181–2186.

[23] N. Ravi, H.-H. Liao, A. F. Jungkunz, A. Widd, and J. C. Gerdes, "Model predictive control of HCCI using variable valve actuation and fuel injection," *Control Eng. Pract.*, vol. 20, no. 4, pp. 421–430, 2012.

[24] C.-J. Chiang and A. G. Stefanopoulou, "Stability analysis in homogeneous charge compression ignition (HCCI) engines with high dilution," *IEEE Trans. Control Syst. Technol.*, vol. 15, no. 2, pp. 209–219, Mar. 2007.

[25] C. S. Daw, R. M. Wagner, K. D. Edwards, and J. B. Green, Jr., "Understanding the transition between conventional spark-ignited combustion and HCCI in a gasoline engine," *Proc. Combustion Inst.*, vol. 31, no. 2, pp. 2887–2894, 2007.

[26] A. Kulzer, D. Lejsek, A. Kiefer, and A. Hettinger, "Pressure trace analysis methods to analyze combustion features and cyclic variability of different gasoline combustion concepts," SAE Tech. Papers 2009-01-0501, 2009.

[27] M. Shahbakhti and C. R. Koch, "Characterizing the cyclic variability of ignition timing in a homogeneous charge compression ignition engine fuelled with *n*-heptane/iso-octane blend fuels," *Int. J. Engine Res.*, vol. 9, no. 5, pp. 361–397, 2008.

[28] E. Hellström, J. Larimore, A. Stefanopoulou, J. Sterniak, and L. Jiang, "Quantifying cyclic variability in a multicylinder HCCI engine with high residuals," *J. Eng. Gas Turbines Power*, vol. 134, no. 11, pp. 112803-1–112803-8, 2012.

[29] A. F. Jungkunz, H.-H. Liao, N. Ravi, and J. C. Gerdes, "Combustion phasing variation reduction for late-phasing HCCI through cycle-to-cycle pilot injection timing control," in *Proc. ASME Dyn. Syst. Control Conf.*, 2011, pp. 685–692, paper DSCC2011-6091.

[30] L. Manofsky, J. Vavra, D. N. Assanis, and A. Babajimopoulos, "Bridging the gap between HCCI and SI: Spark-assisted compression ignition," SAE Tech. Paper 2011-01-1179, 2011.

[31] E. Hellström *et al.*, "Understanding the dynamic evolution of cyclic variability at the operating limits of HCCI engines with negative valve overlap," *SAE Int. J. Engines*, vol. 5, no. 3, pp. 995–1008, 2012.
[32] C.-J. Chiang, C.-C. Chou, and J.-H. Lin, "Adaptive control of homogeneous charge compression ignition (HCCI) engines," in *Proc. Amer. Control Conf. (ACC)*, Jun. 2012, pp. 2066–2071.
[33] C. Nesbit and J. K. Hedrick, "Adaptive engine control," in *Proc. Amer. Control Conf.*, Jun. 1991, pp. 2072–2076.
[34] K. R. Muske, J. C. P. Jones, and E. M. Franceschi, "Adaptive analytical model-based control for SI engine air–fuel ratio," *IEEE Trans. Control Syst. Technol.*, vol. 16, no. 4, pp. 763–768, Jul. 2008.
[35] R. C. Turin and H. Geering, "Model-reference adaptive A/F-ratio control in an SI engine based on Kalman-filtering techniques," in *Proc. Amer. Control Conf.*, vol. 6. Jun. 1995, pp. 4082–4090.
[36] J. Xiaohong and S. Tielong, "Lyapunov-design of adaptive air–fuel ratio control for gasoline engines based on mean-value model," in *Proc. 30th Chin. Control Conf. (CCC)*, Jul. 2011, pp. 6146–6150.
[37] A. M. Frith, C. R. Gent, and A. J. Beaumont, "Adaptive control of gasoline engine air-fuel ratio using artificial neural networks," in *Proc. 4th Int. Conf. Artif. Neural Netw.*, Jun. 1995, pp. 274–278.
[38] S. Jade, E. Hellström, A. Stefanopoulou, and L. Jiang, "On the influence of composition on the thermally-dominant recompression HCCI combustion dynamics," in *Proc. ASME Dyn. Syst. Control Conf.*, 2011, pp. 677–684.
[39] S. Jade, E. Hellström, L. Jiang, and A. G. Stefanopoulou, "Fuel governor augmented control of recompression HCCI combustion during large load transients," in *Proc. Amer. Control Conf.*, Montréal, QC, Canada, Jun. 2012, pp. 2084–2089.
[40] B. J. Allison and A. J. Isaksson, "Design and performance of mid-ranging controllers," *J. Process Control*, vol. 8, nos. 5–6, pp. 469–474, Oct./Dec. 1998.
[41] B. J. Allison and S. Ogawa, "Design and tuning of valve position controllers with industrial applications," *Trans. Inst. Meas. Control*, vol. 25, no. 1, pp. 3–16, Mar. 2003.
[42] M. Karlsson, K. Ekholm, P. Strandh, R. Johansson, P. Tunestål, and B. Johansson, "Closed-loop control of combustion phasing in an HCCI engine using VVA and variable EGR," in *Proc. 5th IFAC Symp. Adv. Automotive Control*, 2007, pp. 501–508.
[43] J. Larimore, S. Jade, E. Hellström, A. G. Stefanopoulou, J. Vanier, and L. Jiang, "Online adaptive residual mass estimation in a multicylinder recompression HCCI engine," in *Proc. ASME Dyn. Syst. Control Conf.*, Palo Alto, CA, USA, 2013, pp. V003T41A005-1–V003T41A005-9.
[44] G. C. Goodwin and K. S. Sin, *Adaptive Filtering Prediction and Control* (Information and System Sciences). Englewood Cliffs, NJ, USA: Prentice-Hall, 1984, ch. 3, sec. 3.3.
[45] Y. Yildiz, A. M. Annaswamy, D. Yanakiev, and I. Kolmanovsky, "Spark-ignition-engine idle speed control: An adaptive control approach," *IEEE Trans. Control Syst. Technol.*, vol. 19, no. 5, pp. 990–1002, Sep. 2011.
[46] M. Voicu, Ed. *Advances in Automatic Control* (Engineering and Computer Science). Norwell, MA, USA: Kluwer, 2004.

Jacob Larimore (S'11) received the bachelor's degree from the Missouri University of Science and Technology, Rolla, MO, USA, in 2009, and the master's and Ph.D. degrees from the University of Michigan, Ann Arbor, MI, USA, in 2012 and 2014, respectively, all in mechanical engineering.

He is currently a Systems Engineer in Systems and Advanced Engineering with Gasoline Systems North America, Robert Bosch LLC, Farmington Hills, MI, USA. His current research interests include modeling and control of advanced internal combustion engines and embedded control systems.

Shyam Jade (S'11) received the bachelor's degree from IIT Bombay, Mumbai, India, in 2009, and the master's and Ph.D. degrees from the University of Michigan, Ann Arbor, MI, USA, in 2011 and 2014, respectively, all in mechanical engineering.

He is currently a Systems Engineer in Systems and Advanced Engineering with Gasoline Systems North America, Robert Bosch LLC, Farmington Hills, MI, USA. His current research interests include modeling and control development for advanced vehicle powertrain systems.

Erik Hellström (M'11) received the M.Sc. degree in applied physics and electrical engineering and the Ph.D. degree from Linköping University, Linköping, Sweden, in 2005 and 2010, respectively.

He was a Research Fellow and Research Scientist with the University of Michigan, Ann Arbor, MI, USA, from 2011 to 2013. He is currently a Research Engineer with Ford Research and Advanced Engineering, Dearborn, MI, USA. His current research interests include modeling, control, and optimal control of vehicle powertrains.

Dr. Hellström is a member of the American Society of Mechanical Engineers and the Society of Automotive Engineers. He is currently an Associate Editor of *Control Engineering Practice*.

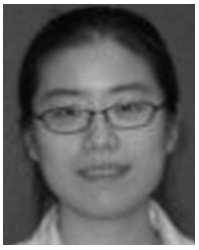

Li Jiang received the bachelor's degree in mechanical engineering from Shanghai Jiao Tong University, Shanghai, China, and the master's degree in electrical system engineering and the Ph.D. degree in mechanical engineering from the University of Michigan, Ann Arbor, MI, USA.

She is currently the Manager in Advanced and System Engineering with Gasoline Systems North America, Robert Bosch LLC, Farmington Hills, MI, USA, where she leads control system development for engine management system applications. She is also the Co-Principal Investigator of Bosch and the U.S. Department of Energy joint research projects on Advanced Combustion Concepts—Enabling Systems and Solutions.

Anna G. Stefanopoulou (S'93–M'96–M'05–F'09) was an Assistant Professor with the University of California at Santa Barbara, Santa Barbara, CA, USA, from 1998 to 2000, and a Technical Specialist with Ford Motor Company, Dearborn, MI, USA, from 1996 to 1997. She is currently a Professor of Mechanical Engineering with the University of Michigan, Ann Arbor, MI, USA, and the Director of the Automotive Research Center, Ann Arbor, a university-based U.S. Army Center of Excellence in Modeling and Simulation of Ground Vehicles. She has co-authored a book entitled *Control of Fuel Cell Power Systems*, authored over 200 publications on estimation and control of internal combustion engines and electrochemical processes, such as fuel cells and batteries, and holds 10 U.S. patents.

Ms. Stefanopoulou is a fellow of the American Society of Mechanical Engineers, the Inaugural Chair of the ASME DSCD Energy Systems Technical Committee, a member of the SAE Dynamic System Modeling Standards Committee, and a member of the U.S. National Academies Committee on Vehicle Fuel Economy Standards.